Physica Medica xxx (2017) xxx–xxx

Contents lists available at ScienceDirect

Physica Medica

journal homepage: http://www.physicamedica.com

Review paper

MRI-guided lung SBRT: Present and future developments

Martin J. Menten, Andreas Wetscherek, Martin F. Fast *

Joint Department of Physics at The Institute of Cancer Research and The Royal Marsden NHS Foundation Trust, London, UK

ARTICLE INFO

Article history:
Received 4 October 2016
Received in Revised form 25 January 2017
Accepted 7 February 2017
Available online xxxx

Keywords:
Lung cancer
SBRT
Hypo-fractionation
MRI guidance
Adaptive radiotherapy

ABSTRACT

Stereotactic body radiotherapy (SBRT) is rapidly becoming an alternative to surgery for the treatment of early-stage non-small cell lung cancer patients. Lung SBRT is administered in a hypo-fractionated, conformal manner, delivering high doses to the target. To avoid normal-tissue toxicity, it is crucial to limit the exposure of nearby healthy organs-at-risk (OAR).

Current image-guided radiotherapy strategies for lung SBRT are mostly based on X-ray imaging modalities. Although still in its infancy, magnetic resonance imaging (MRI) guidance for lung SBRT is not exposure-limited and MRI promises to improve crucial soft-tissue contrast. Looking beyond anatomical imaging, functional MRI is expected to inform treatment decisions and adaptations in the future.

This review summarises and discusses how MRI could be advantageous to the different links of the radiotherapy treatment chain for lung SBRT: diagnosis and staging, tumour and OAR delineation, treatment planning, and inter- or intrafractional motion management. Special emphasis is placed on a new generation of hybrid MRI treatment devices and their potential for real-time adaptive radiotherapy.

Contents

1. Introduction

1.1. The clinical rationale for lung SBRT

Lung cancer is the most common type of cancer, with non-small cell lung cancer (NSCLC) representing the majority of cases [1,2]. Within this patient cohort, roughly 15–20% present with an early and localised form of the disease (stage I), indicating a lack of nodal involvement and metastatic spread. The recent roll-out of wide-scale, low-dose computed tomography (CT)-assisted screening might further increase the number of patients diagnosed at an early disease stage. Traditionally, surgery is the treatment method of choice for these patients [3]. However, some patients are classified as *medically inoperable* due to comorbidities, or they decline surgery for other reasons.

* Corresponding author at: Department of Radiation Oncology, Netherlands Cancer Institute, Amsterdam, The Netherlands.
E-mail addresses: martin.menten@icr.ac.uk (M.J. Menten), m.fast@nki.nl (M.F. Fast).

http://dx.doi.org/10.1016/j.ejmp.2017.02.003
1120-1797/

Please cite this article in press as: Menten MJ et al. MRI-guided lung SBRT: Present and future developments. Phys. Med. (2017), http://dx.doi.org/10.1016/j.ejmp.2017.02.003

In the past, the alternative treatment option of prescribing conventionally fractioned radiotherapy resulted in worse outcome compared to surgery, mainly due to the lack of local control [4]. Taking heed from cranial radiosurgery, stereotactic body radiotherapy (SBRT) aims at delivering fewer, but more intense radiotherapy fractions (hypo-fractionation). Several studies have shown that increasing the biologically effective dose above 100 Gy decreases the number of patients with local failures and increases overall survival in early-stage NSCLC patients compared to conventionally fractionated radiotherapy [5], leading to SBRT being the new standard of care for inoperable early-stage NSCLC patients.

Traditionally, only patients with tumours located at least 2 cm away from the proximal bronchial tree are considered for SBRT [6]. This pre-selection of eligible patients intends to minimise bronchial toxicities, but it also severely limits treatment options for inoperable early-stage NSCLC patients with more centrally located tumours [7]. More recently, trials were set up to identify a slightly milder form of hypo-fractionation suitable for these patients [8]. Furthermore, SBRT is being investigated for the treatment of oligometastatic lung cancer [9,10] and small cell lung cancer [11].

1.2. Current clinical workflow for lung SBRT

While SBRT aims at delivering high doses to the target, it is crucial to limit the exposure of nearby healthy organs-at-risk (OAR), including surrounding lung tissue, the brachial plexus, spinal cord, trachea, proximal bronchial tree, oesophagus, heart and great aortic vessels, liver and ribs [12]. An additional challenge for the radiotherapy of lung tumours are inter- and intrafractional anatomical changes [13].

After diagnosis, staging and treatment decision, the clinical radiotherapy workflow begins with the acquisition of a planning CT scan. Accurate delineation of the tumour and nearby OAR in this image is crucial, as a treatment plan is created based on these contours. Today, many institutions utilise modern delivery techniques for SBRT, such as intensity-modulated radiotherapy and volumetric-modulated arc radiotherapy [14–16]. In conjunction with inverse treatment plan optimization it is possible to design highly conformal dose distributions, even in inhomogeneous anatomies [17,18].

In order to ensure correct delivery of the treatment plan, utmost attention is paid to precise patient positioning for each fraction, for example by using body frames for fixation [19]. About 10–15 years ago, volumetric X-ray imaging started being integrated with modern linear accelerators (linacs) [20–22]. Utilising the provided imaging information, the patient can be rigidly shifted to position the target inside the treatment beam [23,24]. Implanted fiducials often support this process. In addition to rigid shifts, the patient's body may deform between fractions due to weight loss, tumour growth or shrinkage, or volume changes of healthy organs. The volumetric images acquired prior to each fraction can be used to evaluate whether the original treatment plan is still suitable after interfractional motion. If not, a substitute plan can be created, either based on a newly acquired simulation CT scan or using the in-room images themselves [25,26].

Intrafractional motion during treatment delivery, such as respiratory and cardiac movement, may cause the anatomy to shift or deform up to several centimetres [13]. Using a 4D CT scan for treatment planning allows the consideration of breathing motion by deploying either an internal target volume (ITV), mid-ventilation or mid-position approach [27–29]. However, all these methods are based on extended treatment margins and the characteristics of the target motion can change over the course of the treatment [30]. Breathing protocols attempt to reproduce a certain anatomical state during treatment delivery by having the patient hold its breath, either voluntarily [31] or aided by an active breathing control device [32]. Gating turns off the treatment beam if the target leaves a previously defined volume [33]. Both these strategies result in an increased treatment time and reduced patient comfort. More advanced techniques aim at adapting the treatment in real-time by either moving the entire linac [34], tilting the treatment head [35], repositioning the patient using a robotic treatment couch [36,37], or by changing the treatment beam's position and shape by moving the leaves of the linac's multi-leaf collimator (MLC) [38–40]. Most of these techniques have been used to deliver real-time adapted lung SBRT [41–43]. They all require real-time information about the patient's anatomy. This can be obtained by monitoring either internal or external surrogates and correlating them with the tumour motion [44]. The tumour can also be localised using MV portal imaging [45,46] or kV fluoroscopy [47,48]. Automated localisation is often aided by fiducial markers, surgically inserted in or near the target. Another marker-based method detects implanted resonant circuits using an electromagnetic array [49].

1.3. MRI-guided lung SBRT

Despite these advances in lung SBRT delivery technique, there are still residual uncertainties. MRI offers better soft-tissue contrast than CT or cone-beam CT (CBCT), does not expose the patient to additional imaging dose, and offers a larger variety of functional imaging capabilities. For this reason, there has been an increased interest in harnessing MRI for radiotherapy of different cancer sites, including lung. This has the potential to enhance several aspects of the lung SBRT workflow, including:

- diagnosis and staging (Section 3.1),
- delineation of the tumour and OAR for treatment planning (Section 3.2),
- accurate patient setup and adaptation of the treatment to interfractional anatomy changes (Section 3.3),
- monitoring of intrafractional motion and real-time adaptation of the delivery (Section 3.4).

Decreasing the uncertainties in these areas allows shrinking the treatment margins while maintaining dose coverage of the target. Consequently, reduced toxicities in normal-tissue for lung SBRT, and, ultimately, the expansion of the SBRT to more central lung tumours can be surmised.

This review first introduces the various technical implementations of MRI scanners into the radiotherapy workflow (Section 2). Afterwards, it discusses the different areas where MRI is already enhancing lung SBRT treatments or might do so in the future (Section 3). It is important to keep in mind that MRI-guided lung SBRT is still in its infancy and that the number of directly related publications is therefore limited.

2. Technical implementations of MRI scanners into the radiotherapy workflow

2.1. Offline MRI

To employ MRI for diagnostic, staging and treatment simulation purposes, having a stand-alone MRI scanner at the same institution can suffice. However, when using MRI for patient setup and interfractional treatment adaptation, identical patient positioning during imaging and treatment becomes crucial. One way to ensure this relies on the transport of the patient between linac and MRI scanner, located in different rooms, on a trolley system using a shared table top and immobilisation device (see Fig. 1) [50,51].

Please cite this article in press as: Menten MJ et al. MRI-guided lung SBRT: Present and future developments. Phys. Med. (2017), http://dx.doi.org/10.1016/j.ejmp.2017.02.003

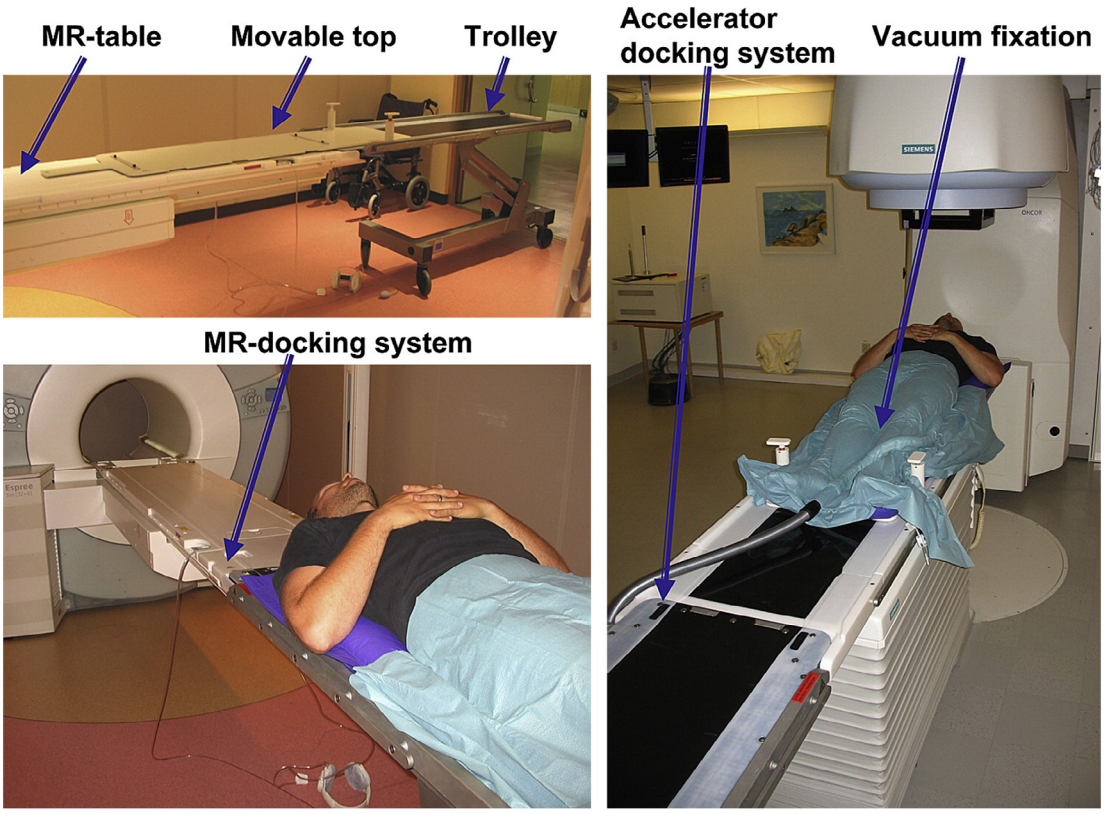

Fig. 1. Three photographs of the shuttle-based MRI-guided radiotherapy solution at Umeå University, Sweden. A movable treatment table and patient fixation system can be attached to either imaging or treatment device. Reprinted from International Journal of Radiation Oncology*Biology*Physics, 74(2), M. Karlsson, M.G. Karlsson, T. Nyholm, C. Amies, B. Zackrisson, Dedicated Magnetic Resonance Imaging in the Radiotherapy Clinic, pp. 644–51, Copyright (2009), with permission from Elsevier.

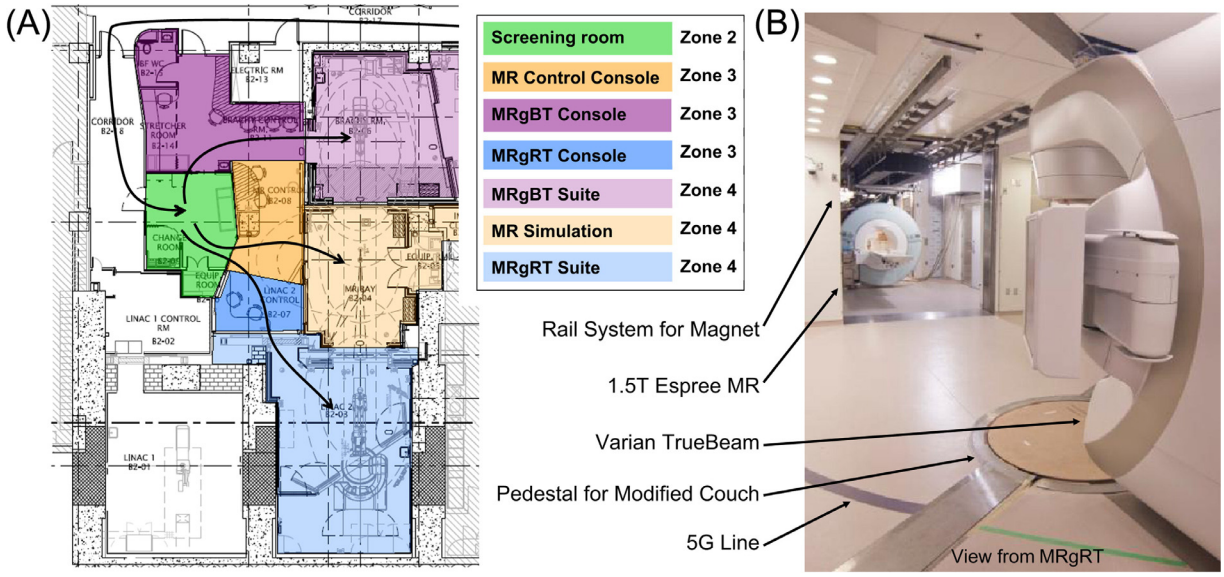

Fig. 2. (A) Floor plan of the MRI-guided facility at Princess Margaret Hospital, Toronto, Canada. (B) The MRI-scanner is attached to rails on the ceiling and can be moved either into the brachytherapy or radiotherapy suite prior to treatment. Reprinted from Seminars in Radiation Oncology, 24(3), D.A. Jaffray, M.C. Carlone, M.F. Milosevic, S.L. Breen, T. Stanescu, A. Rink, H. Alasti, A. Simeonov, M.C. Sweitzer, J.D. Winter, A Facility for Magnetic Resonance–Guided Radiation Therapy, pp. 193–95, Copyright (2014), with permission from Elsevier.

Another option is to shuttle the MRI scanner on ceiling-mounted rails into and out of the treatment room (see Fig. 2) [52]. Both system designs ensure that the magnitude of electromagnetic cross-interference is reduced to a minimum by using spatial separation.

2.2. Online MRI

Offline MRI solutions cannot monitor intrafractional anatomical changes and the patient might move between imaging and

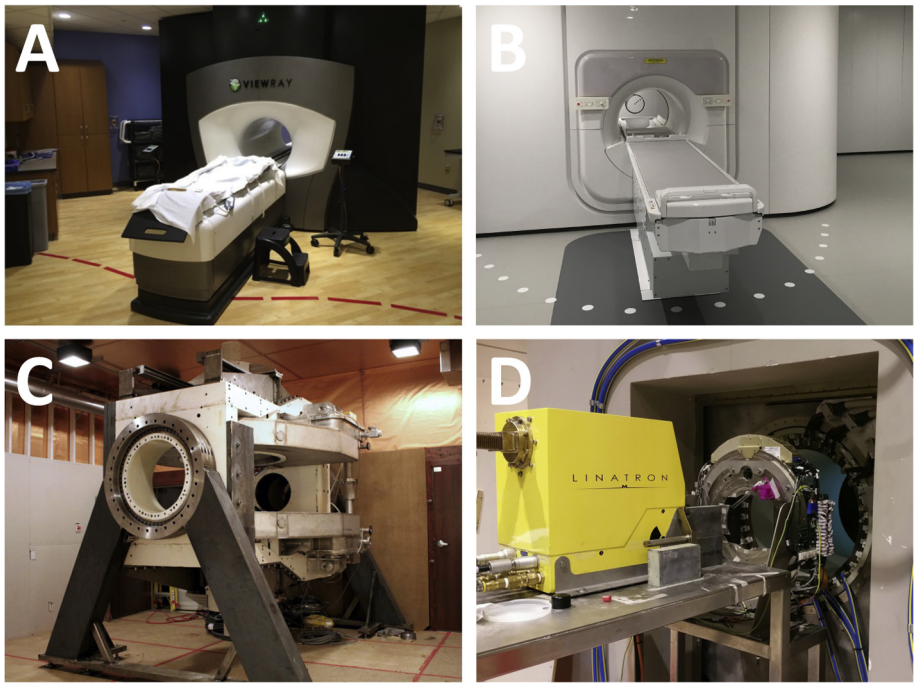

Fig. 3. MRI-guided treatment units developed by different research groups/vendors. (A) The ViewRay MRIdian, the first clinical system at Washington University, St. Louis, MO, USA (image courtesy of P.J. Parikh), (B) the 1.5 T MR-linac developed by Elekta AB installed at NKI-AvL, Amsterdam, The Netherlands, (C) the linac-MR prototype (v1) at Cross Cancer Institute, Edmonton, Canada (image courtesy of B.G. Fallone, www.linacMR.ca), and (D) the MRI-linac prototype developed by the Australian MR-linac program, located at the Ingham Institute, Liverpool, Australia (image courtesy of G.P. Liney on behalf of the Australian MRI-Linac Program).

treatment. For this reason, there are considerable efforts to integrate MRI directly with the treatment unit.

The first commercially available MRI-guided treatment system, based on irradiation with three ^{60}Co sources, has been developed by ViewRay Inc., Cleveland, OH, USA [53]. The system has been used to treat patients since early 2014, including lung cancer patients with SBRT [54]. Several research groups/vendors have been working on combining a linac with MRI (see Fig. 3) [55–58].

Machine design has to warrant correct functioning of both imaging and treatment system in the presence of electromagnetic cross-interference. The choice of beam source and main magnet as well as the orientation and movement of all the components relative to each other directly influences the dose delivery and imaging capabilities. There are considerable differences between systems with regard to treatment beam properties, such as beam energy, penumbra, field-of-view and MLC leaf width at isocenter, and the strength and orientation of the main magnetic field (see Table 1). In addition to beam properties, the dose delivered to the patient is affected by the B_0 magnetic field, which is present at all times. While the primary photon beam is not influenced, the Lorentz force deflects secondary electrons onto a curved trajectory. This electron return effect (ERE) is more pronounced at higher B_0 field strengths and distorts the dose especially at air-tissue-interfaces, which present themselves manifold in thoracic anatomy [59]. Signal- and contrast-to-noise ratio as well as spatial fidelity of the images are affected by the strength and homogeneity of the B0 magnetic field as these govern the relaxation times of the MRI signal. Due to lung tissue's inherently low T2* relaxation time, lower field strengths can be beneficial when attempting to image thoracic anatomies [60].

3. Opportunities for MRI to enhance the lung SBRT workflow

Table 2 provides an overview of the most commonly employed sequences for lung MRI. The table is condensed from the recommendations in [63,64] and annotated with radiotherapy application in mind. Fast spin echo (FSE) sequences are typically acquired using respiratory gating, which is prone to artefacts caused by irregular breathing or cardiac motion. Balanced steady-state free precession (bSSFP) sequences exhibit a T2/T1-weighted contrast and a high signal-to-noise ratio, but can suffer from banding artefacts in peripheral areas of the image, which is problematic if body contours are needed for treatment planning. The traditional limitations of diffusion-weighted (DW) MRI could be overcome by moving away from the echoplanar imaging readout to a segmented readout scheme [65].

3.1. Diagnosis and staging

In order to be eligible for lung SBRT, patients must present at an early disease stage, meaning that only small, localised lesions are

Table 1
System characteristics of the most common hybrid MRI radiotherapy machines. B_0 orientation is specified relative to the treatment beam direction.

Treatment unit	Treatment beam(s)	Magnet design	B_0 [T]	B_0 orientation	Additional comments
ViewRay MRIdian [53]	Three ^{60}Co sources	Split	0.35	Perpendicular	Replacement of ^{60}Co sources with a linac under development
Elekta MR-linac [55]	7 MV linac	Closed	1.5	Perpendicular	Beam traverses cryostat and magnet
Canadian linac-MR (v2) [61]	6 or 10 MV linac	Split	0.5	Inline	Magnet rotates with gantry
Australian MRI-linac [57]	4 or 6 MV linac	Split	1.0*	Inline or perpendicular	Both B_0 orientations under investigation

* The current research version uses a 1.5 T closed magnet [62].

Please cite this article in press as: Menten MJ et al. MRI-guided lung SBRT: Present and future developments. Phys. Med. (2017), http://dx.doi.org/10.1016/j.ejmp.2017.02.003

Table 2
MRI sequences for lung cancer imaging (adapted from [63,64]).

Sequence	Strength	Acquisition type	Spatial resolution	Distortion risk	Variants	Comments
Volumetric T1w GRE	Nodules	Breath-hold	High	Low	Dixon, 4D	Low contrast
T2w single-shot FSE	Infiltrative disease	Breath-hold	Low – moderate	Low	Cine	–
T2w gated FSE	Mediastinal structures, infiltrative disease	Respiratory gated	Moderate – high	Moderate	Dixon, volumetric	Long acquisitions
T2/T1w bSSFP	Lung function	Free-breathing	Moderate – high	Moderate	Cine, 4D	Banding artefacts
T1w FSE	Mediastinal lymph nodes	Multiple breath-hold	Moderate	Moderate	DCE	–
DWI	Dose painting	Multiple breath-hold	Low	High	–	Distortion risk reduction possible

Abbreviations: GRE = gradient echo; DCE = dynamic contrast-enhanced; FSE = fast spin echo; T1w/ T2w = T1/ T2-weighted; bSSFP = balanced steady-state free precession; DWI = diffusion-weighted imaging.

existant without any nodal or metastatic spread. Currently, combined multi-slice CT and ^{18}Fludeoxyglucose (FDG) positron emission tomography (PET), in addition to biopsies, are considered the gold standard for staging [66]. However, biopsy procedures pose an additional burden to the patient and their execution is challenging for small, peripheral tumours [3]. Although the use of PET-CT is well established, the relatively low spatial resolution and motion artefacts, resulting from long acquisition times, are prevalent issues [67,68]. Furthermore, inflammatory areas in the lung can lead to increased FDG uptake and the diagnosis of false positives. MRI could play a role in staging [69,70] and MRI-derived motion information in hybrid PET-MRI devices could be used to mitigate PET motion artefacts [71,72].

In order to determine size and extent of tumour growth with MRI, a range of acquisition techniques has been deployed, for example standard T1- or T2-weighted acquisitions, 2D cine MRI, or single-shot FSE MRI [73,74]. T2-weighted, dynamic contrast-enhanced (DCE), or DW MRI have proven promising in their ability to distinguish between benign and malignant tumours [75–78].

Identifying disease spread to lymph nodes is difficult using PET-CT due to its limited spatial resolution [68]. Several MRI sequences have been investigated to stage mediastinal and hilar lymph node metastases [79–81]. A recent meta-analysis of twelve studies has concluded that MRI offers an improved sensitivity and accuracy over PET-CT [82].

It remains to be seen whether MRI can complement the ubiquitous FDG-PET for diagnosis and staging of lesions. The higher spatial resolution of MRI could prove beneficial for staging and detection of smaller nodes and metastases that could go undetected in PET-CT.

3.2. Delineation, dose calculation and treatment planning

Currently, treatment simulation for lung SBRT is mostly based on CT images. The introduction of PET-CT for target definition has led to a significant decline in delineation uncertainties compared to CT-only contouring [83]. It remains to be seen whether the introduction of MRI for target delineation purposes will result in any additional benefit. Delineation uncertainties are larger for OAR as CT features relatively poor soft-tissue contrast (see Fig. 4), resulting in uncertainties of up to a few centimetres for the oesophagus and spinal cord [84]. The improved soft-tissue contrast of MRI may lead to a reduction in contouring variability for these structures.

When using MRI for treatment planning purposes, it is crucial to ensure spatial fidelity of the image data [85]. One potentially critical issue is the local differences in tissue susceptibility that can induce geometric distortions. For lung tissue, this effect can result in maximum distortions of up to 4 mm, depending on main magnetic field strength, orientation and gradient field strength [86]. However, mean geometric distortions were found to be substantially lower ($\leqslant$1 mm). It should be noted that these errors are in addition to other distortions induced by non-linearities in the main magnetic and gradient field. Recently, the composite 4D distortion effect induced by scanner and susceptibility distortions was investigated for mobile lung tumours of different sizes [87]. Composite distortions were considered manageable ($\leqslant$1 mm), even for high-field MRI scanners as long as these were operated in combination with high readout bandwidth at the cost of increased noise [88]. While not available on all vendor platforms, non-cartesian k-space trajectories, such as a radial or PROPELLER acquisition, can be employed for robustness against motion artefacts [89,90].

Similarly to 4D CT and 4D CBCT – albeit not as established – 4D MRI can be used to evaluate periodic anatomical changes due to breathing. 4D MRI can be either obtained based on repeated acquisition of slices covering the whole volume and respiratory cycle [91–93] or using a continuous 3D acquisition with sophisticated reconstruction techniques [94–96]. While 4D MRI based on 2D acquisitions is more easily available, the 3D-based techniques offer higher resolution and allow for a full 3D distortion correction.

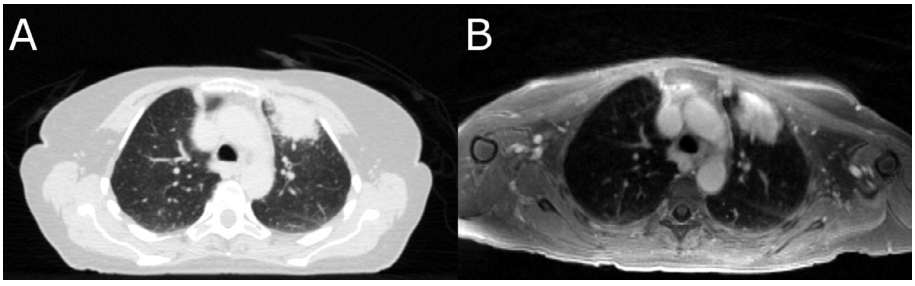

Fig. 4. (A) CT image and (B) T1-weighted MR image acquired with an ultra-fast gradient echo sequence of a NSCLC patient with a tumour located in the left upper lobe. While the bones and lung tissue are better recognizable on the CT image, the soft-tissue contrast of the MR image is superior, especially with respect to the mediastinum.

Please cite this article in press as: Menten MJ et al. MRI-guided lung SBRT: Present and future developments. Phys. Med. (2017), http://dx.doi.org/10.1016/j.ejmp.2017.02.003

A conceptual limitation of 4D scans is that they average over several respiratory cycles and thus cannot accurately depict baseline shifts of breathing motion [97,30]. MRI could be utilised to acquire 2D cine MR images that provide a better visualisation of the patient's breathing, especially with regard to irregularities. Combining 4D MRI with 2D cine MRI using a PCA-based approach allows generation of 3D deformable vector fields with a temporal resolution of 476 ms [93]. In the future, this temporally resolved observation of the tumour motion could be used to define adequate treatment margins.

One obstacle for the widespread introduction of MRI for treatment planning is the absence of electron density and attenuation coefficient information in the MR images. Commonly, this lack of information is circumvented by either generating synthetic (referred to as *pseudo* from here on) CT images from MR images employing Dixon methods, or by (deformably or rigidly) registering the MR image to a treatment planning CT. The accuracy of the latter approach depends on the quality of the registration. While the generation of pseudo-CT images works well for relatively homogeneous treatment sites, such as prostate or brain [98], it is more problematic in the thoracic region, where both lung and bone feature very little MR signal. Correctly accounting for bone and lung tissue during treatment planning is key for achieving the desired dose distribution in the patient. With very limited published data available for thoracic anatomies – one exception being a study on ten patients using a segmentation/bulk density overwrite method [99] – further investigations are necessary to establish the feasibility of pseudo-CT images for treatment planning in lung cancer. Useful experiences may be gained from research on PET-MRI scanners, where electron density information is needed to correctly account for attenuation [100].

Several groups have investigated the influence of the electron return effect on MRI-guided lung SBRT treatments [101–106]. Although machine specifications, magnetic field orientations and strengths differ in these studies, all have found that the dose is distorted by the magnetic field, especially at air-tissue-interfaces in lung and skin. However, dedicated dose calculation algorithms, which are based either on Monte Carlo methods or on solving of the linear Boltzmann transport equation, are able to account for the presence of magnetic fields [107–109]. Several studies have shown that using such dose calculation algorithms to account for the ERE during treatment plan optimization allows for the design of clinically acceptable lung SBRT treatments [104–106].

In hybrid MRI treatment machines the magnetic field also affects machine and treatment plan quality assurance (QA) procedures as the ERE influences the readings of ionization chambers, solid state detectors and radiosensitive films [110–112]. Awareness of the dependence of the detector readout on its orientation relative to the magnetic field, as well as the use of dedicated detectors and phantoms are necessary for dosimetry inside a magnetic field [113–116]. Furthermore, gel-based dosimeters and a shift towards software-based QA procedures are being investigated on MRI-guided treatment units [117,118]. An electronic portal imaging device integrated with the hybrid MRI treatment unit could also be used for treatment beam QA [119].

Functional MRI offers the promise of identifying regions of the tumour that would benefit from additional dose (*boosting* or *dose painting*). While DCE MRI is expected to correlate with the oxygenation level of the tumour, DW MRI could indicate regions of increased tumour cell density [120]. Functional MRI can also identify critical OAR substructures and help minimizing dose to these. For example, for pancoast tumours DW MRI can be used to localise the brachial plexus [121]. Lung ventilation can be assessed with a variety of gaseous contrast agents [122], among which hyperpolarised ^{3}He was employed to identify well-ventilated, healthy parts of the lung for OAR sparing in advanced NSCLC [123]. ^{129}Xe has also been used to assess lung function in NSCLC patients [124] and is more widely available than ^{3}He, but maximal hyperpolarisation is lower [122]. Due to its solubility in blood, ^{129}Xe could enable assessment of gas exchange [125]. A competing method that does not use hyperpolarized gases has emerged in Fourier decomposition MRI, which promises simultaneous characterisation of lung perfusion and ventilation [126]. It can be employed for functional lung avoidance mapping [127], but is free from the infrastructural requirements associated with the application of hyperpolarised noble gases.

MRI has the potential to improve OAR delineation accuracy and may allow functional evaluation of healthy tissue. It remains to be seen whether target delineation in early-stage NSCLC patients treated with SBRT will benefit from MRI, where the tumour is typically very localised with only limited involvement in adjacent soft-tissue. Issues affecting treatment planning arise from MR images not inherently containing electron density information and, on hybrid MRI treatment devices, the B_0 magnetic field distorting the dose distribution and thereby affecting treatment planning and QA procedures. While the latter issue can be accounted for with dedicated dose calculation algorithms and QA protocols, the generation of pseudo CTs for the thoracic region is still under investigation.

3.3. Patient setup and interfractional adaptations

On conventional linacs accurate patient setup is often achieved by shifting the treatment couch based on the position of the lung tumour as derived from an average or 4D CBCT [128]. Using MRI-guided delivery systems, this workflow could be replicated using 3D or 4D MR images. Potential advantages of MRI are the improved soft-tissue contrast and a larger field-of-view resulting in superior discrimination of soft-tissue structures [129].

It should also be noted that on hybrid MRI treatment machines, the ability to apply couch corrections is usually limited to the superior-inferior direction due to the restricted bore dimensions [130]. To correct for shifts in other directions or rotations, the treatment plan segments are morphed according to the position of the target immediately prior to treatment. To validate the safety of this relatively simple plan adaptation, the dose needs to be (re-) calculated on the anatomy of the day. For flattening-filter-free beams, large target shifts can introduce systematic dose deviations compared to the original treatment plan due to the sloped nature of the beam profile [131]. Compensation for this may require more complex adaptations of segment shapes and weights.

A more advanced method aims at generating a treatment plan based on the observed anatomy of the day using the initial simulation treatment plan as a starting point (*warm-start optimization*) [131,132]. This requires a physician, or otherwise trained member of the treatment team to check the contours, which were automatedly deformed onto the daily MR image from the treatment planning CT/MR. Re-delineation may be necessary following visual assessment [10]. This approach minimises computational costs and is expected to mitigate some of the issues related to quality control and plan approval. In the future, full re-planning based on the daily MR image (*cold-start optimization*) might result in even better plan quality.

The use of MRI in order to account for interfractional anatomical changes has just recently gained traction with the emergence of systems allowing MRI near or inside the treatment room. The development and automation of workflows that adapt the treatment plan to the anatomy of the day is increasingly being investigated with clinical outcome results not being available yet.

3.4. Intrafractional motion management

In the past, different methods to monitor intrafractional lung tumour motion have been developed, each with their own

Please cite this article in press as: Menten MJ et al. MRI-guided lung SBRT: Present and future developments. Phys. Med. (2017), http://dx.doi.org/10.1016/j.ejmp.2017.02.003

individual shortcomings. Internal or external surrogates do not necessarily correlate with the target motion and their relation may change over the course of a fraction [133,134,97]. Invasive marker-based localisation methods pose an additional burden to the patient. Additionally, marker migration as well as induced pneumonia have been reported [42]. Neither surrogates, nor marker-based methods are able to monitor nearby OAR or deformations of the target. Markerless tumour or OAR localisation with X-ray imaging is limited by poor soft-tissue contrast [135,136]. All X-ray based imaging methods result in an additional dose to the patient.

The promise of continuously monitoring the tumour as well as nearby healthy organs with high soft-tissue contrast MR images was a strong driving force behind the development of MRI-guided treatment units. For real-time adaptive radiotherapy systems, which adjust the delivery after detecting a change in tumour position, the AAPM Task Group report 76 recommends a total system latency of less than 500 ms [13]. Currently, it is not feasible to acquire, reconstruct and post-process 3D MR images with sufficient resolution and signal-to-noise-ratio in this time frame. MRI allows acquisition of navigator echoes and use of them as a motion surrogate [137]. Visualisation of fast moving lung tumours is therefore usually based on 2D cine acquisition techniques, especially bSSFP sequences. Strategies to further increase the imaging rate have been investigated. Several techniques are based on an undersampled acquisition of the k-space data and subsequent reconstruction of the missing data using compressed sensing or viewsharing [138,139]. Others have deployed motion prediction to create a new image through extrapolation at a rate higher then the imaging frequency [140]. While coils with more than 30 individual channels are commercially available on standard clinical MRI scanners, equivalent hardware still needs to be developed for MRI-guided delivery systems. These enable advanced parallel imaging techniques [141,142] and simultaneous multi-slice imaging [143].

Fig. 5. An MR image acquired on the ViewRay system of a patient undergoing SBRT for oligometastatic cancer in the thorax at Siteman Cancer Center, St. Louis, USA. Continuous sagital cine imaging allows automated localization of the gross tumour volume (inner contour) and gating of the treatment beam if the planning target volume leaves the gating boundary (outer contour). Image courtesy of P.J. Parikh.

Several groups have shown that it is feasible to localise lung tumours in these images using template matching [144,97,145]. More advanced algorithms deploy artificial neural networks [144,146], scale-invariant feature transforms [147,148], or particle filtering [149] to quickly delineate the tumour in each image. The orientation of these 2D imaging planes with respect to the tumour motion can be freely set and even altered during image acquisition. Studies have looked at different strategies to optimise the positioning of these planes to determine kidney or liver tumour motion [150,151], but are yet to be extended to monitoring of lung tumours. Additionally, 4D patient models built based on 4D pretreatment scans may be updated using MR images acquired during delivery [152].

The acquired real-time imaging information can support automated gating of the treatment beam on MRI-guided treatment units (see Fig. 5) [153,154]. Proof-of-concept MLC tracking has been implemented on MRI-linac prototypes [137,155]. Besides not prolonging the treatment time like gating, MLC tracking could adapt the beam aperture to tumour deformations monitored with MRI [156]. It has been shown that the presence of a magnetic field does not hinder the effectiveness of MLC tracking, which is able to reduce exposure of healthy lung tissue when compared to an ITV approach [104].

A stream of volumetric imaging information may also be used for (real-time) dose reconstruction for online quality assurance purposes [157]. Ultimately, real-time images and dosimetric information might be used to adapt the treatment plan during delivery itself, for example after the completion of each treatment beam, treatment segment or even in real-time [158]. In addition to an up-to-date 3D patient dataset, this requires ultra-fast dose calculation algorithms [107,159,160] and treatment plan optimisation strategies [161–163].

Intrafractional tumour and OAR monitoring using MRI might be able to overcome some of the shortcomings of systems based on X-ray imaging, electromagnetic markers or surrogates. However, hybrid MRI treatment devices allowing real-time MRI of the patient undergoing treatment are just becoming available. As of today, intrafractional treatment monitoring and adaptation – MRI-based or not – are only being put into practice by few institutions world-wide and most technologies described in this section are still in a research phase.

4. Conclusion and outlook

This review has highlighted elements of the clinical workflow where the integration of MRI may enhance the quality of lung SBRT. It is expected that MRI will contribute most in the areas of OAR delineation, patient setup, online motion monitoring and plan adaptations. As for most disease sites, the exploitation of MRI for lung radiotherapy is rather new. Therefore, it remains to be seen how far the technical realisation, refinement and integration into the clinical workflow can progress.

Ultimately, it has to be proven whether these conceptual advantages translate into any measurable increase in patient survival or reduction of treatment toxicities, which warrant the additional financial cost of MRI. As it stands, the 5-year absence of local recurrences for early-stage NSCLC patients being treated with lung SBRT is approximately 90% – an already very high value that rivals that of surgery, the current treatment method of choice.

If the integration of MRI is able to substantially increase delivery accuracy and, consequently, allow for higher dose conformality due to treatment margin reduction, it may be possible to deliver higher biologically effective doses to more centrally located lung

Please cite this article in press as: Menten MJ et al. MRI-guided lung SBRT: Present and future developments. Phys. Med. (2017), http://dx.doi.org/10.1016/j.ejmp.2017.02.003

tumours. Even though there has been an interest to deliver SBRT to patients affected by these tumours, dose escalation has often been limited by normal-tissue toxicities.

Acknowledgements

The Institute of Cancer Research is part of the Elekta Atlantic MR-linac Research Consortium and we acknowledge financial and technical support from Elekta AB under a research agreement. Research at The Institute of Cancer Research is supported by Cancer Research UK under Programme C33589/A19727. Dr. Fast is supported by Cancer Research UK under Programme C33589/A19908. We acknowledge NHS funding to the NIHR Biomedical Research Centre at The Royal Marsden and The Institute of Cancer Research.

References

[1] Molina JR, Yang P, Cassivi SD, Schild SE, Adjei AA. Non-small cell lung cancer: epidemiology, risk factors, treatment, and survivorship. Mayo Clin Proc 2008;83(5):584–94. http://dx.doi.org/10.4065/83.5.584.

[2] Ferlay J, Soerjomataram I, Dikshit R, Eser S, Mathers C, Rebelo M, et al. Cancer incidence and mortality worldwide: sources, methods and major patterns in GLOBOCAN 2012. Int J Cancer 2015;136(5):E359–86. http://dx.doi.org/10.1002/ijc.29210.

[3] Vansteenkiste J, De Ruysscher D, Eberhardt WEE, Lim E, Senan S, Felip E, et al. Early and locally advanced non-small-cell lung cancer (NSCLC): ESMO clinical practice guidelines for diagnosis, treatment and follow-up. Ann Oncol 2013;24(suppl 6):vi89–98. http://dx.doi.org/10.1093/annonc/mdt241.

[4] Kaskowitz L, Graham MV, Emami B, Halverson KJ, Rush C. Radiation therapy alone for stage I non-small cell lung cancer. Int J Radiat Oncol Biol Phys 1993;27(3):517–23. http://dx.doi.org/10.1016/0360-3016(93)90374-5.

[5] Guckenberger M. Dose and fractionation in stereotactic body radiation therapy for stage I non-small cell lung cancer: Lessons learned and where do we go next? Int J Radiat Oncol Biol Phys 2015;93(4):765–8. http://dx.doi.org/10.1016/j.ijrobp.2015.08.025.

[6] Timmerman R, Paulus R, Galvin J, Michalski J, Straube W, Bradley J, et al. Stereotactic body radiation therapy for inoperable early stage lung cancer. JAMA 2010;303(11):1070–6. http://dx.doi.org/10.1001/jama.2010.261.

[7] Timmerman R, McGarry R, Yiannoutsos C, Papiez L, Tudor K, et al. Excessive toxicity when treating central tumors in a phase II study of stereotactic body radiation therapy for medically inoperable early-stage lung cancer. J Clin Oncol 2006;24(30):4833–9. http://dx.doi.org/10.1200/JCO.2006.07.5937.

[8] Chang JY, Bezjak A, Mornex F. Stereotactic ablative radiotherapy for centrally located early stage non-small-cell lung cancer: what we have learned. J Thoracic Oncol 2015;10(4):577–85. http://dx.doi.org/10.1097/JTO.0000000000000453.

[9] Norihisa Y, Nagata Y, Takayama K, Matsuo Y, Sakamoto T, Sakamoto M, Mizowaki T, Yano S, Hiraoka M. Stereotactic body radiotherapy for oligometastatic lung tumors. Int J Radiat Oncol Biol Phys 2008;72(2):398–403. http://dx.doi.org/10.1016/j.ijrobp.2008.01.002.

[10] Henke L, Kashani R, Yang D, Zhao T, Green O, Olsen L, et al. Simulated online adaptive magnetic resonance guided stereotactic body radiation therapy for the treatment of oligometastatic disease of the abdomen and central thorax: characterization of potential advantages. Int J Radiat Oncol Biol Phys 2016;96(5):1078–86. http://dx.doi.org/10.1016/j.ijrobp.2016.08.036.

[11] Shioyama Y, Nagata Y, Komiyama T, Takayama K, Shibamoto Y, Ueki N, et al. Multi-institutional retrospective study of stereotactic body radiation therapy for stage I small cell lung cancer: Japan radiation oncology study group (JROSG). Int J Radiat Oncol Biol Phys 2015;93(3):S101. http://dx.doi.org/10.1016/j.ijrobp.2015.07.243.

[12] Kong FM, Ritter T, Quint DJ, Senan S, Gaspar LE, Komaki RU, et al. Consideration of dose limits for organs at risk of thoracic radiotherapy: atlas for lung, proximal bronchial tree, esophagus, spinal cord, ribs, and brachial plexus. Int J Radiat Oncol Biol Phys 2011;81(5):1442–57.

[13] Keall PJ, Mageras GS, Balter JM, Emery RS, Forster KM, Jiang SB, et al. The management of respiratory motion in radiation oncology report of AAPM task group 76. Med Phys 2006;33(10):3874–900. http://dx.doi.org/10.1118/1.2349696.

[14] Verbakel WF, Senan S, Cuijpers JP, Slotman BJ, Lagerwaard FJ. Rapid delivery of stereotactic radiotherapy for peripheral lung tumors using volumetric intensity-modulated arcs. Radiother Oncol 2009;93(1):122–4. http://dx.doi.org/10.1016/j.radonc.2009.05.020.

[15] Navarria P, Ascolese AM, Mancosu P, Alongi F, Clerici E, Tozzi A, et al. Volumetric modulated arc therapy with flattening filter free (FFF) beams for stereotactic body radiation therapy (SBRT) in patients with medically inoperable early stage non small cell lung cancer (NSCLC). Radiother Oncol 2013;107(3):414–8. http://dx.doi.org/10.1016/j.radonc.2013.04.016.

[16] Rossi MM, Peulen HM, Belderbos JS, Sonke JJ. Intrafraction motion in stereotactic body radiation therapy for non-small cell lung cancer: Intensity modulated radiation therapy versus volumetric modulated arc therapy. Int J Radiat Oncol Biol Phys 2016;95(2):835–43. http://dx.doi.org/10.1016/j.ijrobp.2016.01.060.

[17] Ong CL, Palma D, Verbakel WF, Slotman BJ, Senan S. Treatment of large stage I-II lung tumors using stereotactic body radiotherapy (SBRT): planning considerations and early toxicity. Radiother Oncol 2010;97(3):431–6. http://dx.doi.org/10.1016/j.radonc.2010.10.003.

[18] Giglioli FR, Strigari L, Ragona R, Borzi GR, Cagni E, Carbonini C, et al. Lung stereotactic ablative body radiotherapy: a large scale multi-institutional planning comparison for interpreting results of multi-institutional studies. Phys Med 2016;32(4):600–6. http://dx.doi.org/10.1016/j.ejmp.2016.03.015.

[19] Nagata Y, Negoro Y, Aoki T, Mizowaki T, Takayama K, Kokubo M, et al. Clinical outcomes of 3D conformal hypofractionated single high-dose radiotherapy for one or two lung tumors using a stereotactic body frame. Int J Radiat Oncol Biol Phys 2002;52(4):1041–6. http://dx.doi.org/10.1016/S0360-3016(01)02731-6.

[20] Mackie TR, Balog J, Ruchala K, Shepard D, Aldridge S, Fitchard E, et al. Tomotherapy. Semin Radiat Oncol 1999;9(1):108–17. http://dx.doi.org/10.1016/S1053-4296(99)80058-7.

[21] Jaffray DA, Siewerdsen JH, Wong JW, Martinez AA. Flat-panel cone-beam computed tomography for image-guided radiation therapy. Int J Radiat Oncol Biol Phys 2002;53(5):1337–49. http://dx.doi.org/10.1016/S0360-3016(02)02884-5.

[22] Pouliot J, Bani-Hashemi A, Josephine C, Svatos M, Ghelmansarai F, Mitschke M, et al. Low-dose megavoltage cone-beam CT for radiation therapy. Int J Radiat Oncol Biol Phys 2005;61(2):552–60. http://dx.doi.org/10.1016/j.ijrobp.2004.10.011.

[23] Purdie TG, Bissonnette JP, Franks K, Bezjak A, Payne D, Sie F, et al. Cone-beam computed tomography for on-line image guidance of lung stereotactic radiotherapy: localization, verification, and intrafraction tumor position. Int J Radiat Oncol Biol Phys 2007;68(1):243–52. http://dx.doi.org/10.1016/j.ijrobp.2006.12.022.

[24] Sonke JJ, Rossi M, Wolthaus J, van Herk M, Damen E, Belderbos J. Frameless stereotactic body radiotherapy for lung cancer using four-dimensional cone beam CT guidance. Int J Radiat Oncol Biol Phys 2009;74(2):567–74. http://dx.doi.org/10.1016/j.ijrobp.2008.08.004.

[25] Di Y, Frank V, John W, Alvaro M. Adaptive radiation therapy. Phys Med Biol 1997;42(1):123. http://dx.doi.org/10.1088/0031-9155/42/1/008.

[26] Bhatt AD, El-Ghamry MN, Dunlap NE, Bhatt G, Harkenrider MM, Schuler JC, et al. Tumor volume change with stereotactic body radiotherapy (SBRT) for early-stage lung cancer: evaluating the potential for adaptive SBRT. Am J Clin Oncol 2015;38(1):41–6. http://dx.doi.org/10.1097/COC.0b013e318287bd7f.

[27] Stroom JC, Heijmen BJM. Geometrical uncertainties, radiotherapy planning margins, and the ICRU-62 report. Radiother Oncol 2002;64(1):75–83. http://dx.doi.org/10.1016/S0167-8140(02)00140-8.

[28] Wolthaus JW, Schneider C, Sonke JJ, van Herk M, Belderbos JS, Rossi MM, et al. Mid-ventilation CT scan construction from four-dimensional respiration-correlated CT scans for radiotherapy planning of lung cancer patients. Int J Radiat Oncol Biol Phys 2006;65(5):1560–71. http://dx.doi.org/10.1016/j.ijrobp.2006.04.031.

[29] Wolthaus JW, Sonke JJ, van Herk M, Belderbos JS, Rossi MM, Lebesque JV, et al. Comparison of different strategies to use four-dimensional computed tomography in treatment planning for lung cancer patients. Int J Radiat Oncol Biol Phys 2008;70(4):1229–38. http://dx.doi.org/10.1016/j.ijrobp.2007.11.042.

[30] Takao S, Miyamoto N, Matsuura T, Onimaru R, Katoh N, Inoue T, et al. Intrafractional baseline shift or drift of lung tumor motion during gated radiation therapy with a real-time tumor-tracking system. Int J Radiat Oncol Biol Phys 2016;94(1):172–80. http://dx.doi.org/10.1016/j.ijrobp.2015.09.024.

[31] Kimura T, Matsuura K, Murakami Y, Hashimoto Y, Kenjo M, Kaneyasu Y, et al. CT appearance of radiation injury of the lung and clinical symptoms after stereotactic body radiation therapy (SBRT) for lung cancers: are patients with pulmonary emphysema also candidates for SBRT for lung cancers? Int J Radiat Oncol Biol Phys 2006;66(2):483–91. http://dx.doi.org/10.1016/j.ijrobp.2006.05.008.

[32] Cheung PCF, Sixel KE, Tirona R, Ung YC. Reproducibility of lung tumor position and reduction of lung mass within the planning target volume using active breathing control (ABC). Int J Radiat Oncol Biol Phys 2003;57(5):1437–42. http://dx.doi.org/10.1016/j.ijrobp.2003.08.006.

[33] Shirato H, Shimizu S, Kitamura K, Nishioka T, Kagei K, Hashimoto S, et al. Four-dimensional treatment planning and fluoroscopic real-time tumor tracking radiotherapy for moving tumor. Int J Radiat Oncol Biol Phys 2000;48(2):435–42. http://dx.doi.org/10.1016/S0360-3016(00)00625-8.

[34] Adler Jr JR, Chang SD, Murphy MJ, Doty J, Geis P, Hancock SL. The Cyberknife: a frameless robotic system for radiosurgery. Stereotact Funct Neurosurg 1997;69(1–4):124–8. http://dx.doi.org/10.1159/000099863.

[35] Kamino Y, Takayama K, Kokubo M, Narita Y, Hirai E, Kawawda N, et al. Development of a four-dimensional image-guided radiotherapy system with a gimbaled X-ray head. Int J Radiat Oncol Biol Phys 2006;66(1):271–8. http://dx.doi.org/10.1016/j.ijrobp.2006.04.044.

[36] D'Souza WD, Naqvi SA, Yu CX. Real-time intra-fraction-motion tracking using the treatment couch: a feasibility study. Phys Med Biol 2005;50(17):4021–33. http://dx.doi.org/10.1088/0031-9155/50/17/007.

[37] Wilbert J, Meyer J, Baier K, Guckenberger M, Herrmann C, He R, et al. Tumor tracking and motion compensation with an adaptive tumor tracking system (ATTS): system description and prototype testing. Med Phys 2008;35(9):3911–20. http://dx.doi.org/10.1118/1.2964090.

[38] Keall P, Kini V, Vedam S, Mohan R. Motion adaptive X-ray therapy: a feasibility study. Phys Med Biol 2001;46(1):1. http://dx.doi.org/10.1088/0031-9155/46/1/301.
[39] Tacke MB, Nill S, Krauss A, Oelfke U. Real-time tumor tracking: automatic compensation of target motion using the Siemens 160 MLC. Med Phys 2010;37(2):753. http://dx.doi.org/10.1118/1.3284543.
[40] Fast MF, Nill S, Bedford JL, Oelfke U. Dynamic tumor tracking using the Elekta Agility MLC. Med Phys 2014;41(11):111719. http://dx.doi.org/10.1118/1.4899175.
[41] Nuyttens JJ, van de Pol M. The CyberKnife radiosurgery system for lung cancer. Expert Rev Med Devices 2012;9(5):465–75. http://dx.doi.org/10.1586/erd.12.35.
[42] Matsuo Y, Ueki N, Takayama K, Nakamura M, Miyabe Y, Ishihara Y, et al. Evaluation of dynamic tumour tracking radiotherapy with real-time monitoring for lung tumours using a gimbal mounted linac. Radiother Oncol 2014;112(3):360–4. http://dx.doi.org/10.1016/j.radonc.2014.08.003.
[43] Booth JT, Caillet V, Hardcastle N, O'Brien R, Szymura K, Crasta C, et al. The first patient treatment of electromagnetic-guided real time adaptive radiotherapy using MLC tracking for lung SABR. Radiother Oncol 2016;121(1):19–25. http://dx.doi.org/10.1016/j.radonc.2016.08.025.
[44] Ozhasoglu C, Murphy MJ. Issues in respiratory motion compensation during external-beam radiotherapy. Int J Radiat Oncol Biol Phys 2002;52(5):1389–99. http://dx.doi.org/10.1016/S0360-3016(01)02789-4.
[45] Keall PJ, Todor AD, Vedam SS, Bartee CL, Siebers JV, Kini VR, et al. On the use of EPID-based implanted marker tracking for 4D radiotherapy. Med Phys 2004;31(12):3492–9. http://dx.doi.org/10.1118/1.1812608.
[46] Richter A, Wilbert J, Baier K, Flentje M, Guckenberger M. Feasibility study for markerless tracking of lung tumors in stereotactic body radiotherapy. Int J Radiat Oncol Biol Phys 2010;78(2):618–27. http://dx.doi.org/10.1016/j.ijrobp.2009.11.028.
[47] Shimizu S, Shirato H, Ogura S, Akita-Dosaka H, Kitamura K, Nishioka T, et al. Detection of lung tumor movement in real-time tumor-tracking radiotherapy. Int J Radiat Oncol Biol Phys 2001;51(2):304–10. http://dx.doi.org/10.1016/S0360-3016(01)01641-8.
[48] Cui Y, Dy JG, Sharp GC, Alexander B, Jiang SB. Multiple template-based fluoroscopic tracking of lung tumor mass without implanted fiducial markers. Phys Med Biol 2007;52(20):6229–42. http://dx.doi.org/10.1088/0031-9155/52/20/010.
[49] Balter JM, Wright JN, Newell LJ, Friemel B, Dimmer S, Cheng Y, et al. Accuracy of a wireless localization system for radiotherapy. Int J Radiat Oncol Biol Phys 2005;61(3):933–7. http://dx.doi.org/10.1016/j.ijrobp.2004.11.009.
[50] Karlsson M, Karlsson MG, Nyholm T, Amies C, Zackrisson B. Dedicated magnetic resonance imaging in the radiotherapy clinic. Int J Radiat Oncol Biol Phys 2009;74(2):644–51. http://dx.doi.org/10.1016/j.ijrobp.2009.01.065.
[51] Bostel T, Nicolay NH, Grossmann JG, Mohr A, Delorme S, Echner G, et al. MR-guidance–a clinical study to evaluate a shuttle-based MR-linac connection to provide MR-guided radiotherapy. Radiat Oncol 2014;9(1):1. http://dx.doi.org/10.1186/1748-717X-9-12.
[52] Jaffray DA, Carlone MC, Milosevic MF, Breen SL, Stanescu T, Rink A, et al. A facility for magnetic resonance-guided radiation therapy. Seminars Radiat Oncol 2014;24(3):193–5. http://dx.doi.org/10.1016/j.semradonc.2014.02.012.
[53] Mutic S, Dempsey JF. The ViewRay system: magnetic resonance-guided and controlled radiotherapy. Seminars Radiat Oncol 2014;24(3):196–9. http://dx.doi.org/10.1016/j.semradonc.2014.02.008.
[54] www.viewray.com/press-releases/viewray-announces-world-s-first-patients-treated-using-mri-guided-radiation-therapy (2014), accessed on 20th February 2017.
[55] Lagendijk JJW, Raaymakers BW, Raaijmakers AJE, Overweg J, Brown KJ, Kerkhof EM, et al. MRI/linac integration. Radiother Oncol 2008;86(1):25–9. http://dx.doi.org/10.1016/j.radonc.2007.10.034.
[56] Fallone BG, Murray B, Rathee S, Stanescu T, Steciw S, Vidakovic S, et al. First MR images obtained during megavoltage photon irradiation from a prototype integrated linac-MR system. Med Phys 2009;36(6):2084–8. http://dx.doi.org/10.1118/1.3125662.
[57] Keall PJ, Barton M, Crozier S, on behalf of the Australian MRI-Linac Program, including contributors from Ingham Institute Illawarra Cancer Care Centre Liverpool Hospital Stanford University Universities of Newcastle Queensland Sydney Western Sydney and Wollongong, The Australian magnetic resonance imaging-linac program, Seminars Radiat Oncol 24 (3) (2014) 203–6. doi: http://dx.doi.org/10.1016/j.semradonc.2014.02.015.
[58] Mutic S, Low D, Chmielewski T, Fought G, Hernandez M, Kawrakow I, et al. TU-H-BRA-08: The design and characteristics of a novel compact linac-based MRI guided radiation therapy (MR-IGRT) system. Med Phys 2016;43(6):3770. http://dx.doi.org/10.1118/1.4957630.
[59] Raaijmakers AJ, Raaymakers BW, Lagendijk JJ. Integrating a MRI scanner with a 6 MV radiotherapy accelerator: dose increase at tissue-air interfaces in a lateral magnetic field due to returning electrons. Phys Med Biol 2005;50(7):1363–76. http://dx.doi.org/10.1088/0031-9155/50/7/002.
[60] Wachowicz K, De Zanche N, Yip E, Volotovskyy V, Fallone BG. CNR considerations for rapid real-time MRI tumor tracking in radiotherapy hybrid devices: effects of B0 field strength. Med Phys 2016;43(8):4903–14. http://dx.doi.org/10.1118/1.4959542.
[61] Keyvanloo A, Burke B, Aubin JS, Baillie D, Wachowicz K, Warkentin B, et al. Minimal skin dose increase in longitudinal rotating biplanar linac-MR systems: examination of radiation energy and flattening filter design. Phys Med Biol 2016;61(9):3527.
[62] Liney GP, Dong B, Begg J, Vial P, Zhang K, Lee F, et al. Technical note: experimental results from a prototype high-field inline MRI-linac. Med Phys 2016;43(9):5188–94.
[63] Ohno Y, Koyama H, Dinkel J, Hintze C. Lung cancer. In: Kauczor HU, editor. MRI of the lung. Springer; 2009. p. 179–216.
[64] Biederer J, Beer M, Hirsch W, Wild J, Fabel M, Puderbach M, et al. MRI of the lung (2/3). why when how?, Insights into. Imaging 2012;3(4):355–71. http://dx.doi.org/10.1007/s13244-011-0146-8.
[65] Liney GP, Holloway L, Harthi TMA, Sidhom M, Moses D, Juresic E, et al. Quantitative evaluation of diffusion-weighted imaging techniques for the purposes of radiotherapy planning in the prostate. Br J Radiol 2015;88(1049):20150034. http://dx.doi.org/10.1259/bjr.20150034.
[66] De Ruysscher D, Belderbos J, Reymen B, van Elmpt W, van Baardwijk A, Wanders R, et al. State of the art radiation therapy for lung cancer 2012: a glimpse of the future. Clin Lung Cancer 2013;14(2):89–95. http://dx.doi.org/10.1016/j.cllc.2012.06.006.
[67] Devaraj A, Cook GJ, Hansell DM. PET/CT in non-small cell lung cancer staging-promises and problems. Clin Radiol 2007;62(2):97–108. http://dx.doi.org/10.1016/j.crad.2006.09.015.
[68] Cheebsumon P, Boellaard R, de Ruysscher D, van Elmpt W, van Baardwijk A, Yaqub M, et al. Assessment of tumour size in PET/CT lung cancer studies: PET- and CT-based methods compared to pathology. Eur J Nucl Med Mol Imaging 2012;2(1):1–9. http://dx.doi.org/10.1186/2191-219X-2-56.
[69] Hochhegger B, Marchiori E, Sedlaczek O, Irion K, Heussel C, Ley S, Ley-Zaporozhan J, Souza AS Jr, Kauczor H. MRI in lung cancer: a pictorial essay. Br J Radiol. doi:http://dx.doi.org/10.1259/bjr/24661484.
[70] Cobben DCP, de Boer HCJ, Tijssen RH, Rutten EGGM, van Vulpen M, Peerlings J, et al. Emerging role of MRI for radiation treatment planning in lung cancer. Technol Cancer Res Treat 2016;15(6):NP47–60. http://dx.doi.org/10.1177/1533034615615249.
[71] Rank CM, Heusser T, Wetscherek A, Freitag M, Sedlaczek O, Schlemmer H-P, et al. Respiratory motion compensation for simultaneous PET/MR based on highly undersampled MR data. Med Phys 2016;43(12):6234–45. http://dx.doi.org/10.1118/1.4966128.
[72] Munoz C, Kolbitsch C, Reader AJ, Marsden P, Schaeffter T, Prieto C. MR-based cardiac and respiratory motion-compensation techniques for PET-MR imaging. PET Clinics 2016;11(2):179–91. http://dx.doi.org/10.1016/j.cpet.2015.09.004.
[73] Kajiwara N, Akata S, Uchida O, Usuda J, Ohira T, Kawate N, et al. Cine MRI enables better therapeutic planning than CT in cases of possible lung cancer chest wall invasion. Lung Cancer 2010;69(2):203–8. http://dx.doi.org/10.1016/j.lungcan.2009.10.016.
[74] Chang S, Hong SR, Kim YJ, Hong YJ, Hur J, Choi BW, et al. Usefulness of thin-section single-shot turbo spin echo with half-fourier acquisition in evaluation of local invasion of lung cancer. J Magn Reson Imaging 2015;41(3):747–54. http://dx.doi.org/10.1002/jmri.24587.
[75] Puderbach M, Hintze C, Ley S, Eichinger M, Kauczor HU, Biederer J. MR imaging of the chest: a practical approach at 1.5T. Eur J Radiol 2007;64(3):345–55. http://dx.doi.org/10.1016/j.ejrad.2007.08.009.
[76] Zou Y, Zhang M, Wang Q, Shang D, Wang L, Yu G. Quantitative investigation of solitary pulmonary nodules: dynamic contrast-enhanced MRI and histopathologic analysis. Am J Roentgenol 2008;191(1):252–9. http://dx.doi.org/10.2214/AJR.07.2284.
[77] Ohba Y, Nomori H, Mori T, Ikeda K, Shibata H, Kobayashi H, et al. Is diffusion-weighted magnetic resonance imaging superior to positron emission tomography with fludeoxyglucose F 18 in imaging non-small cell lung cancer? J Thoracic Cardiovasc Surg 2009;138(2):439–45. http://dx.doi.org/10.1016/j.jtcvs.2008.12.026.
[78] Chen L, Zhang J, Bao J, Zhang L, Hu X, Xia Y, et al. Meta-analysis of diffusion-weighted MRI in the differential diagnosis of lung lesions. J Magn Reson Imaging 2013;37(6):1351–8. http://dx.doi.org/10.1002/jmri.23939.
[79] Hasegawa I, Eguchi K, Kohda E, Tanami Y, Mori T, Hatabu H, et al. Pulmonary hilar lymph nodes in lung cancer: assessment with 3D-dynamic contrast-enhanced MR imaging. Eur J Radiol 2003;45(2):129–34. http://dx.doi.org/10.1016/S0720-048X(02)00056-6.
[80] Ohno Y, Hatabu H, Takenaka D, Higashino T, Watanabe H, Ohbayashi C, et al. Metastases in mediastinal and hilar lymph nodes in patients with non–small cell lung cancer: quantitative and qualitative assessment with STIR turbo spin-echo MR imaging 1. Radiology 2004;231(3):872–9. http://dx.doi.org/10.1148/radiol.2313030103.
[81] Nakayama J, Miyasaka K, Omatsu T, Onodera Y, Terae S, Matsuno Y, et al. Metastases in mediastinal and hilar lymph nodes in patients with non-small cell lung cancer: quantitative assessment with diffusion-weighted magnetic resonance imaging and apparent diffusion coefficient. J Comput Assist Tomogr 2010;34(1):1–8. http://dx.doi.org/10.1097/RCT.0b013e3181a9cc07.
[82] Peerlings J, Troost EGC, Nelemans PJ, Cobben DCP, de Boer JCJ, Hoffmann AL, et al. The diagnostic value of MR imaging in determining the lymph node status of patients with nonsmall cell lung cancer: a meta-analysis. Radiology 2016;281(1):86–98. http://dx.doi.org/10.1148/radiol.2016151631.
[83] Steenbakkers RJ, Duppen JC, Fitton I, Deurloo KE, Zijp LJ, Comans EF, et al. Reduction of observer variation using matched CT-PET for lung cancer delineation: a three-dimensional analysis. Int J Radiat Oncol Biol Phys 2006;64(2):435–48. http://dx.doi.org/10.1016/j.ijrobp.2005.06.034.

Please cite this article in press as: Menten MJ et al. MRI-guided lung SBRT: Present and future developments. Phys. Med. (2017), http://dx.doi.org/10.1016/j.ejmp.2017.02.003

[84] Cui Y, Chen W, Olsen LA, Beatty RE, Maxim PG, Ritter T, et al. Contouring variations and the role of atlas in non-small cell lung cancer radiation therapy: analysis of a multi-institutional preclinical trial planning study. Pract Radiat Oncol 2015;5(2):e67–75. http://dx.doi.org/10.1016/j.prro.2014.05.005.
[85] Moerland M, Beersma R, Bhagwandien R, Wijrdeman H, Bakker C. Analysis and correction of geometric distortions in 1.5 T magnetic resonance images for use in radiotherapy treatment planning. Phys Med Biol 1995;40(10):1651. http://dx.doi.org/10.1088/0031-9155/40/10/007.
[86] Stanescu T, Wachowicz K, Jaffray D. Characterization of tissue magnetic susceptibility-induced distortions for MRIgRT. Med. Phys. 2012;39(12):7185–93. http://dx.doi.org/10.1118/1.4764481.
[87] Stanescu T, Jaffray D. Investigation of the 4D composite MR image distortion field associated with tumor motion for MR-guided radiotherapy. Med Phys 2016;43(3):1550–62. http://dx.doi.org/10.1118/1.4941958.
[88] Schmidt MA, Payne GS. Radiotherapy planning using MRI. Phys Med Biol 2015;60(22):R323. http://dx.doi.org/10.1088/0031-9155/60/22/R323.
[89] Block KT, Chandarana H, Milla S, Bruno M, Mulholland T, Fatterpekar F, et al. Towards routine clinical use of radial stack-of-stars 3D gradient-echo sequences for reducing motion sensitivity. J Korean Soc Magn Reson Med 2014;18(2):87–106. http://dx.doi.org/10.13104/jksmrm.2014.18.2.87.
[90] Pipe JG, Gibbs WN, Li Z, Karis JP, Schar M, Zwart NR. Revised motion estimation algorithm for PROPELLER MRI. Magn Reson Med 2014;72(2):430–7. http://dx.doi.org/10.1002/mrm.24929.
[91] Tryggestad E, Flammang A, Han-Oh S, Hales R, Herman J, McNutt T, et al. Respiration-based sorting of dynamic MRI to derive representative 4D-MRI for radiotherapy planning. Med Phys 2013;40(5):051909. http://dx.doi.org/10.1118/1.4800808.
[92] Liu Y, Yin F-F, Czito BG, Bashir MR, Cai J. T2-weighted four dimensional magnetic resonance imaging with result-driven phase sorting. Med Phys 2015;42(8):4460–71. http://dx.doi.org/10.1118/1.4923168.
[93] Stemkens B, Tijssen RHN, de Senneville BD, Lagendijk JJW, van den Berg CAT. Image-driven, model-based 3D abdominal motion estimation for MR-guided radiotherapy. Phys Med Biol 2016;61(14):5335. http://dx.doi.org/10.1088/0031-9155/61/14/5335.
[94] Feng L, Grimm R, Block KT, Chandarana H, Kim S, Xu J, et al. Golden-angle radial sparse parallel MRI: combination of compressed sensing, parallel imaging, and golden-angle radial sampling for fast and flexible dynamic volumetric MRI. Magn Reson Med 2014;72(3):707–17. http://dx.doi.org/10.1002/mrm.24980.
[95] Rank CM, Heuer T, Buzan MTA, Wetscherek A, Freitag MT, Dinkel J, et al. 4D respiratory motion-compensated image reconstruction of free-breathing radial MR data with very high undersampling. Magn Reson Med 2016. http://dx.doi.org/10.1002/mrm.26206.
[96] Mickevicius NJ, Paulson E. Investigation of undersampling and reconstruction algorithm dependence on respiratory correlated 4D-MRI for online MR-guided radiation therapy. Phys Med Biol. doi:http://dx.doi.org/10.1088/1361-6560/aa54f2.
[97] Tryggestad E, Flammang A, Hales R, Herman J, Lee J, McNutt T, et al. 4D tumor centroid tracking using orthogonal 2D dynamic MRI: implications for radiotherapy planning. Med Phys 2013;40(9):091712. http://dx.doi.org/10.1118/1.4818656.
[98] Nyholm T, Jonsson J. Counterpoint: opportunities and challenges of a magnetic resonance imaging-only radiotherapy work flow. Seminars Radiat Oncol 2014;24(3):175–80. http://dx.doi.org/10.1016/j.semradonc.2014.02.005.
[99] Jonsson JH, Karlsson MG, Karlsson M, Nyholm T. Treatment planning using MRI data: an analysis of the dose calculation accuracy for different treatment regions. Radiat Oncol 2010;5(1):1. http://dx.doi.org/10.1186/1748-717X-5-62.
[100] Mehranian A, Arabi H, Zaidi H. Vision 20/20: magnetic resonance imaging-guided attenuation correction in PET/MRI: challenges, solutions, and opportunities. Med Phys 2016;43(3):1130–55. http://dx.doi.org/10.1118/1.4941014.
[101] Kirkby C, Murray B, Rathee S, Fallone BG. Lung dosimetry in a linac-MRI radiotherapy unit with a longitudinal magnetic field. Med Phys 2010;37(9):4722–32. http://dx.doi.org/10.1118/1.3475942.
[102] Yang YM, Geurts M, Smilowitz JB, Sterpin E, Bednarz BP. Monte Carlo simulations of patient dose perturbations in rotational-type radiotherapy due to a transverse magnetic field: a tomotherapy investigation. Med Phys 2015;42(2):715–25. http://dx.doi.org/10.1118/1.4905168.
[103] Oborn B, Ge Y, Hardcastle N, Metcalfe P, Keall P. Dose enhancement in radiotherapy of small lung tumors using inline magnetic fields: a Monte Carlo based planning study. Med Phys 2016;43(1):368–77. http://dx.doi.org/10.1118/1.4938580.
[104] Menten MJ, Fast MF, Nill S, Kamerling CP, McDonald F, Oelfke U. Lung stereotactic body radiotherapy with an MR-linac – quantifying the impact of the magnetic field and real-time tumor tracking. Radiother Oncol 2016;119(3):461–6. http://dx.doi.org/10.1016/j.radonc.2016.04.019.
[105] Merna C, Rwigema J-CM, Cao M, Wang P-C, Kishan AU, Michailian A, et al. A treatment planning comparison between modulated tri-cobalt-60 teletherapy and linear accelerator–based stereotactic body radiotherapy for central early-stage non- small cell lung cancer. Med Dosim 2016;41(1):87–91. http://dx.doi.org/10.1016/j.meddos.2015.09.002.
[106] Park JM, Park SY, Kim HJ, Wu HG, Carlson J, Kim JI. A comparative planning study for lung SABR between tri-Co-60 magnetic resonance image guided radiation therapy system and volumetric modulated arc therapy. Radiother Oncol 2016;120(2):279–85. http://dx.doi.org/10.1016/j.radonc.2016.06.013.
[107] Hissoiny S, Ozell B, Bouchard H, Després P. GPUMCD: a new GPU-oriented Monte Carlo dose calculation platform. Med Phys 2011;38(2):754–64. http://dx.doi.org/10.1118/1.3539725.
[108] St Aubin J, Keyvanloo A, Vassiliev O, Fallone BG. A deterministic solution of the first order linear Boltzmann transport equation in the presence of external magnetic fields. Med Phys 2015;42(2):780–93. http://dx.doi.org/10.1118/1.4905041.
[109] Bouchard H, Bielajew A. Lorentz force correction to the Boltzmann radiation transport equation and its implications for monte carlo algorithms. Phys Med Biol 2015;60(13):4963–71. http://dx.doi.org/10.1088/0031-9155/60/13/4963.
[110] Meijsing I, Raaymakers BW, Raaijmakers AJE, Kok JGM, Hogeweg L, Liu B, Lagendijk JJW. Dosimetry for the MRI accelerator: the impact of a magnetic field on the response of a farmer NE2571 ionization chamber. Phys Med Biol 2009;54(10):2993. http://dx.doi.org/10.1088/0031-9155/54/10/002.
[111] Reynolds M, Fallone BG, Rathee S. Dose response of selected solid state detectors in applied homogeneous transverse and longitudinal magnetic fields. Med Phys 2014;41(9):092103. http://dx.doi.org/10.1118/1.4893276.
[112] Reynoso FJ, Curcuru A, Green O, Mutic S, Das IJ, Santanam L. Technical note: magnetic field effects on Gafchromic-film response in MR-IGRT. Med Phys 2016;43(12):6552–6. http://dx.doi.org/10.1118/1.4967486.
[113] Smit K, van Asselen B, Kok JGM, Aalbers AHL, Lagendijk JJW, Raaymakers BW. Towards reference dosimetry for the MR-linac: magnetic field correction of the ionization chamber reading. Phys Med Biol 2013;58(17):5945. http://dx.doi.org/10.1088/0031-9155/58/17/5945.
[114] Smit K, Sjöholm J, Kok JGM, Lagendijk JJW, Raaymakers BW. Relative dosimetry in a 1.5 T magnetic field: an MR-linac compatible prototype scanning water phantom. Phys Med Biol 2014;59(15):4099. http://dx.doi.org/10.1088/0031-9155/59/15/4099.
[115] Li HH, Rodriguez VL, Green OL, Hu Y, Kashani R, Wooten HO, et al. Patient-specific quality assurance for the delivery of 60Co intensity modulated radiation therapy subject to a 0.35-T lateral magnetic field. Int J Radiat Oncol Biol Phys 2015;91(1):65–72. 0.1016/j.ijrobp.2014.09.008.
[116] van Zijp HM, van Asselen B, Wolthaus JWH, Kok JMG, de Vries JHW, Ishakoglu K, et al. Minimizing the magnetic field effect in MR-linac specific QA-tests: the use of electron dense materials. Phys Med Biol 2016;61(3):N50. http://dx.doi.org/10.1088/0031-9155/61/3/N50.
[117] Alnaghy SJ, Gargett M, Liney G, Petasecca M, Begg J, Espinoza A, et al. Initial experiments with gel-water: towards MRI-linac dosimetry and imaging. Australas Phys Eng Sci Med 2016;39(4):921–32. http://dx.doi.org/10.1007/s13246-016-0495-1.
[118] Chen G-P, Ahunbay E, Li XA. Technical note: development and performance of a software tool for quality assurance of online replanning with a conventional linac or MR-linac. Med Phys 2016;43(4):1713–9. http://dx.doi.org/10.1118/1.4943795.
[119] Raaymakers BW, de Boer JCJ, Knox C, Crijns SPM, Smit K, Stam MK, et al. Integrated megavoltage portal imaging with a 1.5 T MRI linac. Phys Med Biol 2011;56(19):N207. http://dx.doi.org/10.1088/0031-9155/56/19/N01.
[120] van der Heide UA, Houweling AC, Groenendaal G, Beets-Tan RG, Lambin P. Functional MRI for radiotherapy dose painting. Magn Reson Imaging 2012;30(9):1216–23. http://dx.doi.org/10.1016/j.mri.2012.04.010.
[121] Andreou A, Sohaib A, Collins DJ, Takahara T, Kwee TC, Leach MO, et al. Diffusion-weighted MR neurography for the assessment of brachial plexopathy in oncological practice. Cancer Imaging 2015;15(1):6. http://dx.doi.org/10.1186/s40644-015-0041-5.
[122] Biederer J, Heussel CP, Puderbach M, Wielpuetz MO. Functional magnetic resonance imaging of the lung. Seminars Respir Crit Care Med 2014;35(1):74–82. http://dx.doi.org/10.1055/s-0033-1363453.
[123] Ireland RH, Bragg CM, McJury M, Woodhouse N, Fichele S, Van Beek EJ, et al. Feasibility of image registration and intensity-modulated radiotherapy planning with hyperpolarized helium-3 magnetic resonance imaging for non–small-cell lung cancer. Int J Radiat Oncol Biol Phys 2007;68(1):273–81. http://dx.doi.org/10.1016/j.ijrobp.2006.12.068.
[124] Qing K, Mugler J, Chen Q. WE-FG-206-07: assessing the lung function of patients with non-small cell lung cancer using hyperpolarized Xenon-129 dissolved-phase MRI. Med Phys 2016;43(6). http://dx.doi.org/10.1118/1.4957937. 3832-3832.
[125] Driehuys B, Möller HE, Cleveland ZI, Pollaro J, Hedlund LW. Pulmonary perfusion and xenon gas exchange in rats: MR imaging with intravenous injection of hyperpolarized ^{129}Xe. Radiology 2009;252(2):386–93. http://dx.doi.org/10.1148/radiol.2513081550.
[126] Bauman G, Puderbach M, Deimling M, Jellus V, Chefd'hotel C, Dinkel J, et al. Non-contrast-enhanced perfusion and ventilation assessment of the human lung by means of fourier decomposition in proton MRI. Magn Reson Med 2009;62(3):656–64. http://dx.doi.org/10.1002/mrm.22031.
[127] Capaldi D, Sheikh K, Hoover D, Yaremko B, Palma D, Parraga G. TH-CD-202-09: free-breathing proton MRI functional lung avoidance maps to guide radiation therapy. Med Phys 2016;43(6). http://dx.doi.org/10.1118/1.4958165. 3878-3878.
[128] Sonke J-J, Belderbos J. Adaptive radiotherapy for lung cancer. Seminars Radiat Oncol 2010;20(2):94–106. http://dx.doi.org/10.1016/j.semradonc.2009.11.003.
[129] Noel CE, Parikh PJ, Spencer CR, Green OL, Hu Y, Mutic S, et al. Comparison of onboard low-field magnetic resonance imaging versus onboard computed

tomography for anatomy visualization in radiotherapy. Acta Oncol 2015;54 (9):1474–82. http://dx.doi.org/10.3109/0284186X.2015.1062541.
[130] Bol G, Lagendijk J, Raaymakers B. Virtual couch shift (VCS): accounting for patient translation and rotation by online IMRT re-optimization. Phys Med Biol 2013;58(9):2989. http://dx.doi.org/10.1088/0031-9155/58/9/2989.
[131] Ates O, Ahunbay EE, Moreau M, Li XA. Technical note: a fast online adaptive replanning method for VMAT using flattening filter free beams. Med Phys 2016;43(6):2756–64. http://dx.doi.org/10.1118/1.4948676.
[132] Acharya S, Fischer-Valuck BW, Kashani R, Parikh P, Yang D, Zhao T, et al. Online magnetic resonance image guided adaptive radiation therapy: first clinical applications. Int J Radiat Oncol Biol Phys 2016;94(2):394–403. http://dx.doi.org/10.1016/j.ijrobp.2015.10.015.
[133] Korreman SS, Juhler-Nottrup T, Boyer AL. Respiratory gated beam delivery cannot facilitate margin reduction, unless combined with respiratory correlated image guidance. Radiother Oncol 2008;86(1):61–8. http://dx.doi.org/10.1016/j.radonc.2007.10.038.
[134] Malinowski K, McAvoy TJ, George R, Dietrich S, D'Souza WD. Incidence of changes in respiration-induced tumor motion and its relationship with respiratory surrogates during individual treatment fractions. Int J Radiat Oncol Biol Phys 2012;82(5):1665–73. http://dx.doi.org/10.1016/j.ijrobp.2011.02.048.
[135] Dieterich S, Gibbs IC. The CyberKnife in clinical use: current roles, future expectations. IMRT, IGRT, SBRT, vol. 43. Karger Publishers; 2011. p. 181–94.
[136] Menten MJ, Fast MF, Nill S, Oelfke U. Using dual-energy x-ray imaging to enhance automated lung tumor tracking during real-time adaptive radiotherapy. Med Phys 2015;42(12):6987–98. http://dx.doi.org/10.1118/1.4935431.
[137] Crijns SP, Raaymakers BW, Lagendijk JJ. Proof of concept of MRI-guided tracked radiation delivery: tracking one-dimensional motion. Phys Med Biol 2012;57(23):7863–72. http://dx.doi.org/10.1088/0031-9155/57/23/7863.
[138] Yip E, Yun J, Wachowicz K, Heikal AA, Gabos Z, Rathee S, et al. Prior data assisted compressed sensing: a novel MR imaging strategy for real time tracking of lung tumors. Med Phys 2014;41(8):082301. http://dx.doi.org/10.1118/1.4885960.
[139] Lee D, Greer PB, Pollock S, Kim T, Keall P. Quantifying the accuracy of the tumor motion and area as a function of acceleration factor for the simulation of the dynamic keyhole magnetic resonance imaging method. Med Phys 2016;43(5):2639. http://dx.doi.org/10.1118/1.4947508.
[140] Seregni M, Paganelli C, Lee D, Greer PB, Baroni G, Keall PJ, et al. Motion prediction in MRI-guided radiotherapy based on interleaved orthogonal cine-MRI. Phys Med Biol 2016;61(2):872–87. http://dx.doi.org/10.1088/0031-9155/61/2/872.
[141] Wright KL, Harrell MW, Jesberger JA, Landeras L, Nakamoto DA, Thomas S, et al. Clinical evaluation of CAIPIRINHA: comparison against a GRAPPA standard. J Magn Reson Imaging 2014;39(1):189–94. http://dx.doi.org/10.1002/jmri.24105.
[142] Uecker M, Lai P, Murphy MJ, Virtue P, Elad M, Pauly JM, et al. ESPIRiTan eigenvalue approach to autocalibrating parallel MRI: Where SENSE meets GRAPPA. Magn Reson Med 2014;71(3):990–1001. http://dx.doi.org/10.1002/mrm.24751.
[143] Farah R, Park S, Shea S, Tryggestad E, Wong J, Hales R, et al. TH-CD-207A-01: evaluation of lung tumor motion management strategy with dynamic MRI. Med Phys 2016;43(6). http://dx.doi.org/10.1118/1.4958170. 3879-3879.
[144] Cervino LI, Du J, Jiang SB. MRI-guided tumor tracking in lung cancer radiotherapy. Phys Med Biol 2011;56(13):3773–85. http://dx.doi.org/10.1088/0031-9155/56/13/003.
[145] Shi X, Diwanji T, Mooney KE, Lin J, Feigenberg S, D'Souza WD, et al. Evaluation of template matching for tumor motion management with cine-MR images in lung cancer patients. Med Phys 2014;41(5):052304. http://dx.doi.org/10.1118/1.4870978.
[146] Yun J, Yip E, Gabos Z, Wachowicz K, Rathee S, Fallone BG. Neural-network based autocontouring algorithm for intrafractional lung-tumor tracking using linac-MR. Med Phys 2015;42(5):2296–310. http://dx.doi.org/10.1118/1.4916657.
[147] Paganelli C, Lee D, Greer PB, Baroni G, Riboldi M, Keall P. Quantification of lung tumor rotation with automated landmark extraction using orthogonal cine MRI images. Phys Med Biol 2015;60(18):7165–78. http://dx.doi.org/10.1088/0031-9155/60/18/7165.
[148] Mazur TR, Fischer-Valuck BW, Wang Y, Yang D, Mutic S, Li HH. SIFT-based dense pixel tracking on 0.35 T cine-MR images acquired during image-guided radiation therapy with application to gating optimization. Med Phys 2016;43 (1):279. http://dx.doi.org/10.1118/1.4938096.
[149] Bourque AE, Bedwani S, Filion E, Carrier JF. A particle filter based autocontouring algorithm for lung tumor tracking using dynamic magnetic resonance imaging. Med Phys 2016;43(9):5161. http://dx.doi.org/10.1118/1.4961403.
[150] Bjerre T, Crijns S, af Rosenschold PM, Aznar M, Specht L, Larsen R, et al. Three-dimensional MRI-linac intra-fraction guidance using multiple orthogonal cine-MRI planes. Phys Med Biol 2013;58(14). http://dx.doi.org/10.1088/0031-9155/58/14/4943. 4943-4450.
[151] Brix L, Ringgaard S, Srensen T, Poulsen P. Three-dimensional liver motion tracking using real-time two-dimensional MRI. Med Phys 2014;41(4). http://dx.doi.org/10.1118/1.4867859. 042302-042302.
[152] McClelland JR, Blackall JM, Tarte S, Chandler AC, Hughes S, Ahmad S, et al. A continuous 4D motion model from multiple respiratory cycles for use in lung radiotherapy. Med Phys 2006;33(9):3348–58. http://dx.doi.org/10.1118/1.2222079.
[153] Crijns SP, Kok JG, Lagendijk JJ, Raaymakers BW. Towards MRI-guided linear accelerator control: gating on an MRI accelerator. Phys Med Biol 2011;56 (15):4815–25. http://dx.doi.org/10.1088/0031-9155/56/15/012.
[154] Green OP, Goddu S, Mutic S. SU-E-T-352: commissioning and quality assurance of the first commercial hybrid MRI-IMRT system. Med Phys 2012;39(6). http://dx.doi.org/10.1118/1.4735439. 3785-3785.
[155] Yun J, Wachowicz K, Mackenzie M, Rathee S, Robinson D, Fallone BG. First demonstration of intrafractional tumor-tracked irradiation using 2D phantom MR images on a prototype linac-MR. Med Phys 2013;40 (5):051718. http://dx.doi.org/10.1118/1.4802735.
[156] Ge Y, O'Brien RT, Shieh CC, Booth JT, Keall PJ. Toward the development of intrafraction tumor deformation tracking using a dynamic multi-leaf collimator. Med Phys 2014;41(6):061703. http://dx.doi.org/10.1118/1.4873682.
[157] Kamerling CP, Fast MF, Ziegenhein P, Menten MJ, Nill S, Oelfke U. Real-time 4D dose reconstruction for tracked dynamic MLC deliveries for lung SBRT. Med Phys 2016;43(11):6072–81. http://dx.doi.org/10.1118/1.4965045.
[158] Kamerling C, Fast M, Ziegenhein P, Nill S, Oelfke U. TH-CD-202-12: online inter-beam replanning based on real-time dose reconstruction. Med Phys 2016;43(6). http://dx.doi.org/10.1118/1.4958169. 3879-3879.
[159] Jia X, Gu X, Graves YJ, Folkerts M, Jiang SB. GPU-based fast Monte Carlo simulation for radiotherapy dose calculation. Phys Med Biol 2011;56 (22):7017–31. http://dx.doi.org/10.1088/0031-9155/56/22/002.
[160] Ziegenhein P, Pirner S, Ph Kamerling C, Oelfke U. Fast CPU-based Monte Carlo simulation for radiotherapy dose calculation. Phys Med Biol 2015;60 (15):6097–111. http://dx.doi.org/10.1088/0031-9155/60/15/6097.
[161] Bol GH, Hissoiny S, Lagendijk JJ, Raaymakers BW. Fast online Monte Carlo-based IMRT planning for the MRI linear accelerator. Phys Med Biol 2012;57 (5):1375–85. http://dx.doi.org/10.1088/0031-9155/57/5/1375.
[162] Ziegenhein P, Kamerling CP, Bangert M, Kunkel J, Oelfke U. Performance-optimized clinical IMRT planning on modern CPUs. Phys Med Biol 2013;58 (11):3705–15. http://dx.doi.org/10.1088/0031-9155/58/11/3705.
[163] Kontaxis C, Bol GH, Lagendijk JJ, Raaymakers BW. Towards adaptive IMRT sequencing for the MR-linac. Phys Med Biol 2015;60(6):2493–509. http://dx.doi.org/10.1088/0031-9155/60/6/2493.

Please cite this article in press as: Menten MJ et al. MRI-guided lung SBRT: Present and future developments. Phys. Med. (2017), http://dx.doi.org/10.1016/j.ejmp.2017.02.003